RAS M-231

OF FACTOR 12

NEC-JH_66

Fatigue Crack Propagation Rates for Notched 304 Stainless Steel Specimens In Elevated Temperature Water

Gary L. Wire

William J. Mills

Bechtel Bettis, Inc.,
West Mifflin, PA 15122-0079

U.S. NUCLEAR REGULATORY COMMISSION
the Matter of Entergy Nuclear Vermont Yankee LLC
cket No. 50-271 Official Exhibit No. NEC-JH-66
FERED by: Applicant/Licensee Intervenor NEC
NRC Staff Other
ENTIFIED on 7/21/08 Witness/Panel Hopenfeld
ion Taken: ADMITTED REJECTED WITHDRAWN
porter/Clerk MAC

Fatigue crack propagation (FCP) rates for 304 stainless steel (304 SS) were determined in 24°C and 288°C air and 288°C water with 20–60 cc H_2/kg H_2O using double-edged notch (DEN) specimens. Tests performed at matched loading conditions in air and water provided a direct comparison of the relative crack growth rates over a wide range of test conditions. Crack growth rates of 304 SS in water were about 12 times the air rate for both short cracks (0.03–0.25 mm) and long cracks up to 4.06 mm beyond the notch, which are consistent with conventional deep crack tests. The large environmental degradation for 304 SS crack growth is consistent with the strong reduction of fatigue life in high hydrogen water. Further, very similar environmental effects were reported in fatigue crack growth tests in hydrogen water chemistry (HWC). Prior to the recent tests reported by Wire and Mills [1] and Evans and Wire [2], most literature data in high hydrogen water showed only a mild environmental effect for 304 SS, of order 2.5 times air or less. However, the tests were predominantly performed at high cyclic stress intensities or high frequencies where environmental effects are small. The environmental effect in low oxygen environments at low stress intensity depends strongly on both the stress ratio, R, and the load rise time, T_r. Fractographic examinations were performed on specimens tested in both air and water to understand the operative cracking mechanisms associated with environmental effects. In 288°C water, the fracture surfaces were crisply faceted with a crystallographic appearance, and showed striations under high magnification. The cleavage-like facets suggest that hydrogen embrittlement is the primary cause of accelerated cracking. [DOI: 10.1115/1.1767859]

1 Introduction

Fatigue crack propagation data for Type 304 stainless steel (304 SS) were obtained in air and an elevated temperature aqueous environment. The data were developed from instrumented fatigue tests on double-edged notched (DEN) fatigue specimens with two different notch root radii ρ of 0.38 and 1.52 mm, reported by Wire et al. [3]. The fatigue tests were primarily designed to determine the effect of notch radius on fatigue crack initiation but also provide fatigue crack growth data for both shallow and long cracks. Direct comparison of crack growth rates obtained in air and water under identical loading conditions and for equivalent crack sizes demonstrates that 304 SS experiences a large environmental effect, and the detailed analysis below shows that this trend was supported by all tests.

2 Experimental

The DEN specimens (Fig. 1) were machined from a 127 mm diameter bar forging with an L-C orientation per ASTM E1823, with yield and ultimate strength of 288 and 546 MPa. The chemical composition of the 304 SS material is provided in [1]. The microstructure consists of nonsensitized grains with a grain size of ASTM 2.

Load-controlled cyclic fatigue tests were performed in air at room temperature and 288°C and in deaerated 288°C water. The electric potential drop (EPD) technique with current reversal was used to monitor crack initiation and growth, as detailed in [1].

The double-edge notched uniaxial specimen provides two sites for crack initiation. It provides an advantage over compact tension specimens in that it can be tested in both tension-tension and tension-compression loading conditions. Tests were performed under load control in fully reversed ($R=-1$) and tension-tension loading ($R=0$). Alignment was achieved by manually adjusting the pull rod to minimize bending stresses, which were monitored by strain gages attached to the specimen (Fig. 1). Once a satisfactory alignment was achieved, the strain gages were removed and the EPD leads were attached. For the tests in water, the assembly was then enclosed in an autoclave, which was filled with water and heated to 288°C. Deaerated water containing 20 to 60 cc H_2/kg H_2O was used in this study. The room temperature pH was 10.1 to 10.3, and the oxygen concentration was less than 20 ppb. The specimen was cycled until crack initiation was detected, based on the electrical potential drop reading corresponding to a crack growth of 0.13 mm. Following an interim visual inspection, cycling was continued to obtain crack extension data.

The crack growth rate da/dN was calculated using the secant method applied to the average extension curves, as discussed by Wire [1]. Crack growth rates were obtained at extensions as low as 0.013 mm in order to investigate possible short crack effects. For conventional deep cracks, rates were calculated over larger increments of crack extension.

For shallow cracks, of depth $L<\rho$ from the notch, the stress intensity factor solution developed by Schijve [4] for a crack emanating from an edge notch was used to compute K. When the crack depth exceeded the notch root radius, the conventional stress intensity factor solution developed by Tada et al. [5] for DEN specimens, which is based on the total crack depth including the notch depth, was used to calculate K. The transition between the two formulations was made at $L=\rho$. It is noted that an inde-

Contributed by the Pressure Vessels and Piping Division for publication in the JOURNAL OF PRESSURE VESSEL TECHNOLOGY. Manuscript received by the PVP Division May 29, 2003; revision received December 23, 2004. Editor: S. Y. Zamrik.

Copyright © 2004 by ASME

DOCKETED
USNRC

August 12, 2008 (11:00am)

OFFICE OF SECRETARY
RULEMAKINGS AND
ADJUDICATIONS STAFF

Template Secy-028

DS-03

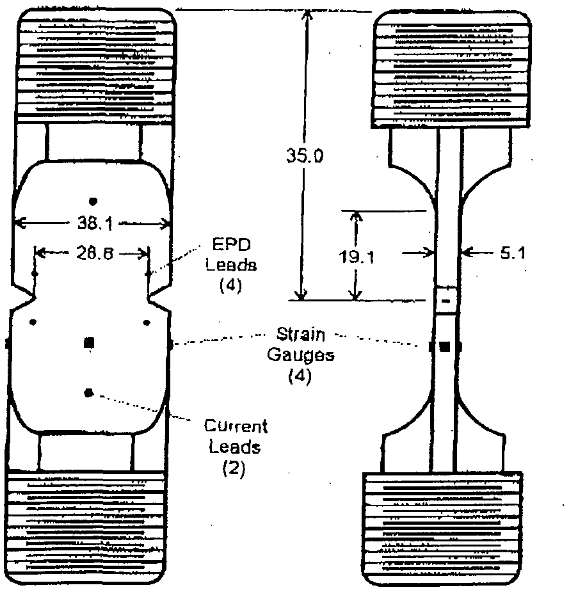

Fig. 1 Double-edge notched fatigue specimen with EPD (Grip details not shown, all dimensions in mm)

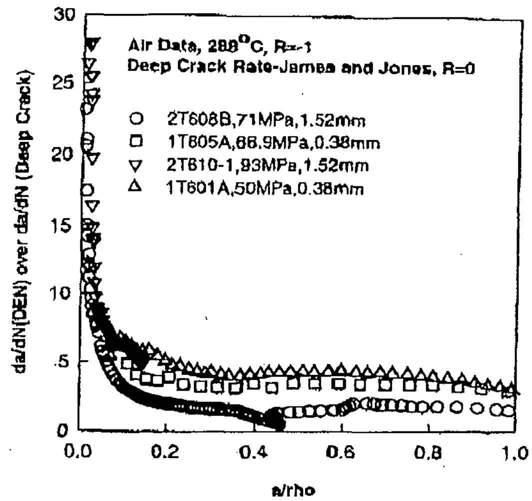

Fig. 2 Short crack growth rates from DEN specimens. Rates normalized by deep crack rates using positive ΔK, Eq. 2

pendent K solution for a double-edge notched plate by Yamamoto [6] provided results within 4% for shallow and intermediate crack lengths over the range of the present tests. For both the fully reversed and tension-tension tests, the stress intensity factor range (ΔK) is defined as the difference between K at maximum and minimum loads (i.e., $\Delta K = K_{max} - K_{min}$). Crack asymmetry is a potential problem with the DEN specimen. However, the largest difference observed between the two cracks was 2 mm out of an overall crack length ($D+L$) of about 9 mm. The 2 mm difference is less than 5% of the specimen width of 38 mm, indicating crack asymmetry is not a problem for this data.

Broken specimen halves were examined on a scanning electron microscope (SEM) to characterize the fatigue fracture surface morphology. The crack length associated with each fractograph was determined so fracture surface features could be correlated with crack growth rates and applied ΔK levels. Relative amounts of α' martensite on fracture faces were estimated using a commercial ferrite measurement instrument (Feritscope® MP3C). While fracture surface roughness and the presence of only a thin layer of martensite precluded precise measurements, relative amounts of martensite were readily determined.

3 Test Results

3.1 Short Crack Effects. Before examining environmental effects, it is appropriate to evaluate the cracking behavior for short versus long cracks. Crack growth rates for short cracks can be much larger than long crack data due to differences in crack closure according to Newman [7]. Crack closure in the crack wake reduces the portion of the load that is effective in growing a crack. However, short cracks have little or no crack wake, and closure is subsequently reduced. To examine for such closure effects, the growth rates in air for the DEN at $R=-1$ were compared directly to growth rates from conventional deep crack tests in air at 288°C, $R=0$ per James and Jones [8]:

$$da/dN = 1.40\times10^{-9}\Delta K^{3.57}, \text{ mm/cycle}, \ \Delta K \text{ in MPa}\sqrt{m} \tag{2}$$

The ratio of the DEN rates to rates for long cracks from Eq. (2) are shown in Fig. 2. It was convenient to use only the positive portion of the loading to calculate the air rates for long cracks, as the ratio in Fig. 2 then decreased to values near unity at large crack depths. The figure shows that the short crack growth rates can exceed the deep crack rates by a factor of thirty, but that the ratio quickly approaches a stable value as the crack depth becomes significant compared to the notch radius. The value of the ratio at larger crack depths ranged from approximately one to four for the tests shown, implying that the tensile portion of the loading is largely responsible for the crack propagation at large crack depths. For the particular notch depths studied here, short crack effects are only important below L/ρ of order 0.2. Therefore, shallow crack effects can produce an order of magnitude increase in crack growth rates under fully reversed loading conditions, but this acceleration is confined to very small crack extensions, on the order of 0.1 to 0.3 mm. For longer cracks, conventional test data for deeply cracked specimens can be used to predict cracking behavior.

The increased rates observed for short cracks near notches is consistent with increased effective stress intensity, as reviewed in depth by Lalor, Sehitoglu, and McClung [9]. They observed that the crack opening stress increased rapidly with increasing crack depth and leveled out for crack depths above approximately 40% of the notch radius. They were able to explain the observed crack opening stresses on the basis of finite element analysis of crack closure effects.

3.2 Environmental Effects by Comparison to Controls. The effect of environment on fatigue crack growth can be seen by directly comparing the data from 288°C air and water tests, as controls were run in air at the same or very similar loading conditions to the tests in water. This allows a direct assessment of environmental effects down to the smallest detectable crack extensions, while avoiding the need for an explicit treatment of short crack effects. Hence, the da/dN values in air and water are compared directly at the same crack extension and cyclic stress. This assures that crack driving forces are the same, without having to explicitly calculate them.

Figure 3 shows conclusively that the crack growth rates in water are much enhanced over rates in air. The ratio of crack growth rates in water over air is called the environmental ratio (ER), for convenience. At a stress amplitude of 69 MPa and lowest frequency tested of 0.0033 Hz, the ER is 15 (Fig. 3(a)). The large ER in water observed in Fig. 3(a) persisted to the end of the test, where the crack extension was 4.1 mm. Hence, large environmental effects continue to crack depths of engineering significance,

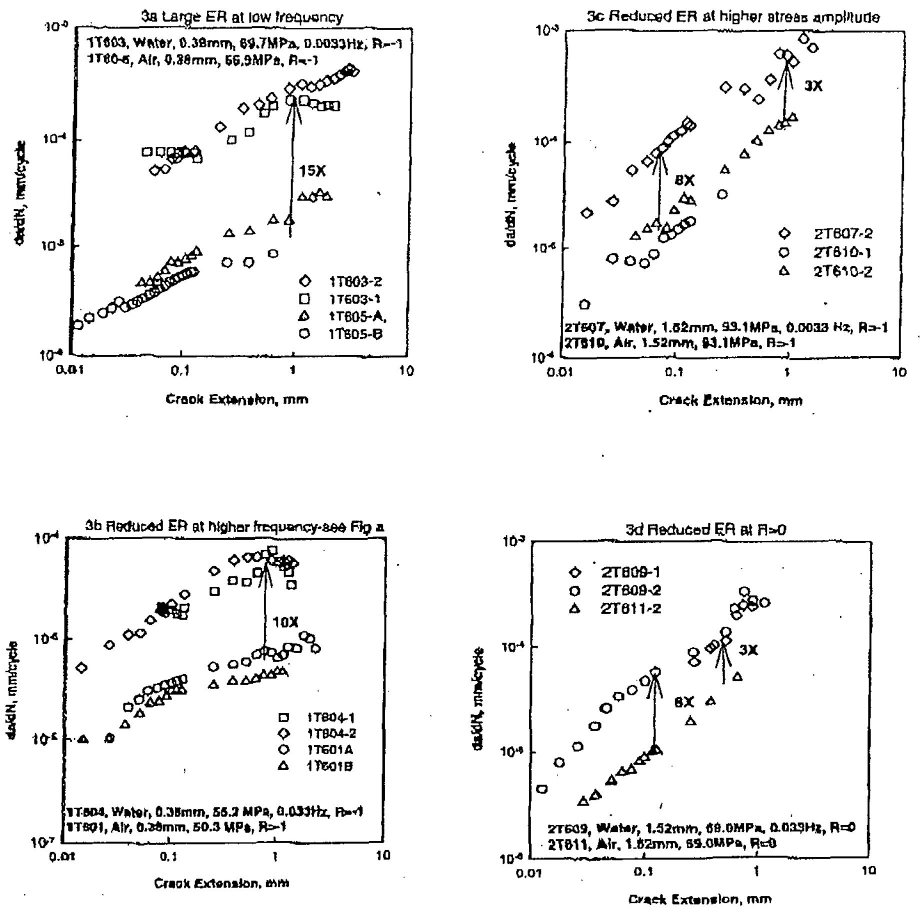

Fig. 3 Environmental effects in DEN tests. Stress amplitude and other test parameters on plots

and are not just a short crack phenomenon. Figure 3 shows that the ER was large at the smallest detectable crack extensions of about 0.025 mm. Hence, the increases in crack growth rate explain the reductions in fatigue life reported in the literature [10].

Several other trends are worthy of note. Higher frequency led to a smaller ER of 10×, as shown by comparing Fig. 3(b) and Fig. 3(a). The apparent increase in ER with decreasing frequency is consistent with the reduction of fatigue life at low strain rate noted by Chopra and Smith [10]. The ER for a higher stress amplitude (Fig. 3(c)) is only about a factor of 8× compared to 15× in Fig. 3(a) at the same low frequency, indicating a reduction in ER at high stress amplitude and crack growth rates. The ER at $R=0$ is also smaller, as shown in Fig. 3(d). This may be further evidence of an effect of higher effective loading for a given stress amplitude provided by $R=0$ compared to $R=-1$, which has a compressive half cycle. Also, the ER in Fig. 3(c,d) decreases at the largest crack extensions, which correspond to the highest stress intensity. Such an effect is consistent with the general notion that at high loading, mechanical effects will dominate.

3.3 Environmental Effects Using Time-Based Plots and Comparison to Literature. From a fundamental point of view, the crack tip strain rate is the appropriate crack driving parameter to correlate environmentally assisted crack propagation rate data, as reviewed by Scott [11]. However, a unique method of crack-tip strain-rate calculation could not be established and variability in calculated values was over a factor of ten between various models. Shoji et al. [12] suggested using the time-based rate in air as a practical correlating parameter representing crack tip strain-rate for low alloy steel fatigue crack growth data. This variable was used successfully to correlate environmental effects on low alloy steels in water. The time-based crack growth in air $(da/dt)_a$ is defined as

$$(da/dt)_a=(da/dN)_{air}/T_r \quad \text{where } T_r \text{ is the load rise time} \tag{3a}$$

and the time based environmental rate $(da/dt)_e$ in water is

$$(da/dt)_e=(da/dN)_e/T_r \tag{3b}$$

Eq. (3) is appropriate for fatigue crack growth tests with continuous cycling, which produce a time-independent rate such as seen in the present tests. In the event that stress corrosion cracking or other time-dependent behavior is operative, the total time would be more appropriate in Eq. 3.

The strong environmental effects observed on 304 SS are correlated reasonably well by utilizing a time-based plot, as shown in Fig. 4, although data variability is large. The air rates for DEN specimens were determined directly from the control tests in air, as shown in Fig. 3. The 304 SS DEN data (diamonds) show a clear increase in crack growth rates relative to those in air at low air rates, and are consistent with the degradation of fatigue life of up to 15× reported by Chopra and Smith [10] and 13× reported by Leax [13]. As noted above, the large ER did not diminish in one test up to a crack depth of 4.1 mm. This depth is greater than associated with "short crack" effects and is significant from an engineering standpoint. Subsequent tests on conventional compact tension specimens at this laboratory, represented by the circles in

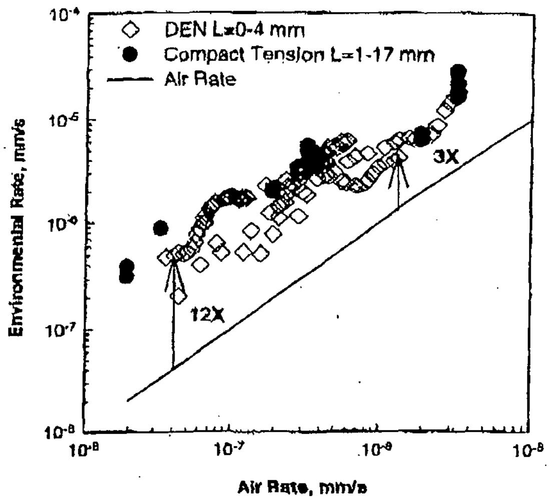

Fig. 4 304 SS DEN crack growth rates in water vs air. Trend shows decreased ER at high air rate. Air rates are calculated directly from control tests

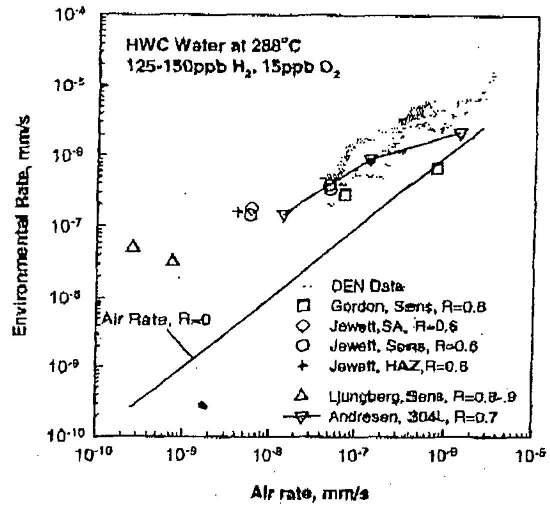

Fig. 6 Comparison of DEN to CT data in HWC Large environmental effects extend to low air rates

Fig. 4, verify that the environmental effect continues unabated to a crack growth of 17 mm, as reported by Evans and Wire [2]. For 304 SS CT data, the baseline crack growth rate in air, $(da/dN)_{air}$, was determined via [8] for the appropriate test conditions (i.e., ΔK, R, and temperature). It is also noted that the agreement between short crack and long crack results indicates that there is no "chemical" enhancement of crack growth of short cracks, such as reported by Gangloff [14] for high strength steel in a NaCl solution.

A review of fatigue crack propagation of austenitic stainless steels was performed recently by Shack and Kassner [15]. Data from surface crack tests performed in low oxygen "hydrogen water chemistry" (HWC) environments by Prater et al. [16] are compared with DEN data in Fig. 5. HWC is BWR water chemistry with hydrogen added to control the electrochemical potential. The literature tests on surface crack specimens tested in HWC water confirm that the large environmental effects shown here have been observed previously. Overall, the surface crack tests from the literature average about 14 times the air rate, very similar to DEN data. Indeed, crack growth rates in HWC at frequencies between 1.67×10^{-2} and 5.56×10^{-4} Hz are identical to those obtained in this study. The fact that the stainless steel studied by Prater was sensitized does not appear to be important, as the cracking mode was transgranular. Gordon et al. [17] indicated that the fatigue crack growth rates in HWC water were the same for solution annealed and sensitized 304 SS, and Jewett et al. [18] reported very similar rates in these materials as well as welds.

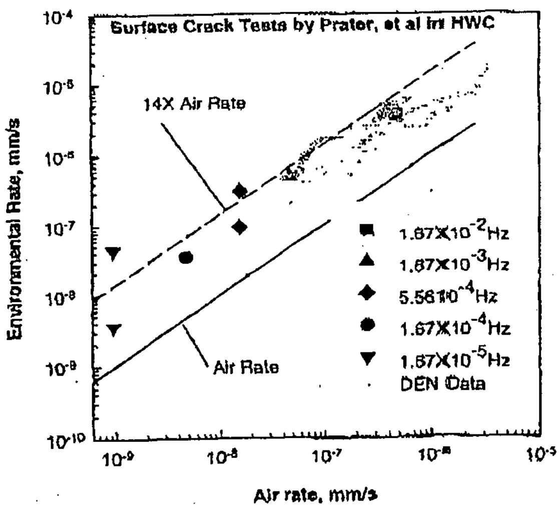

Fig. 5 Comparison of DEN to surface crack data. Surface crack data tested in HWC [16]

A comparison of crack growth data trends from DEN tests and selected conventional compact tension test data in HWC is provided in Fig. 6. The DEN and CT data are in good agreement in the intermediate growth rate regimes where both specimen types were evaluated. Moreover, the data by Ljunberg [19] show even greater enhancement in the low crack growth rate regime. These results provide further support for the observation that environmental effects tend to increase in the lower stress intensity regime where crack growth rates in air are reduced.

The tests by Andresen and Campbell [20] show evidence for a transition to reduced environmental effects at high equivalent air rates, and more limited data by Gordon et al. [17] are consistent with such an effect. It is noteworthy that the DEN data agree qualitatively with HWC data in Fig. 6, including evidence of a transition to substantially lower environmental effects at equivalent air rates above 10^{-6} mm/s.

The hydrogen level for the HWC test data in Figs. 5 and 6 is 150 ppb or less, much less than several ppm in the current DEN tests and in PWR water. Although the corrosion potential in HWC is typically about 0.3 V SHE higher than that in water with higher hydrogen used in the present tests, according to Gilman [21], the overall crack growth rate response in the two environments appears to be similar.

3.4 Effects of Stress Ratio, Stress Intensity, and Rise Time. Evans and Wire [2] performed a series of tests on a 1.9T CT specimen (thickness=24.1 mm) of the same heat and water conditions used in the DEN tests. The CT tests showed that large environmental effects occurred in conventional, deeply cracked compact tension specimens with high hydrogen levels and the attendant lower potential. Results from the DEN tests and the compact tension tests by Evans and Wire (2002) are shown in Fig. 7. For DEN data represented in Figs. 7–8, the full cyclic stress range and crack extensions increments of 0.12 mm or larger were employed.

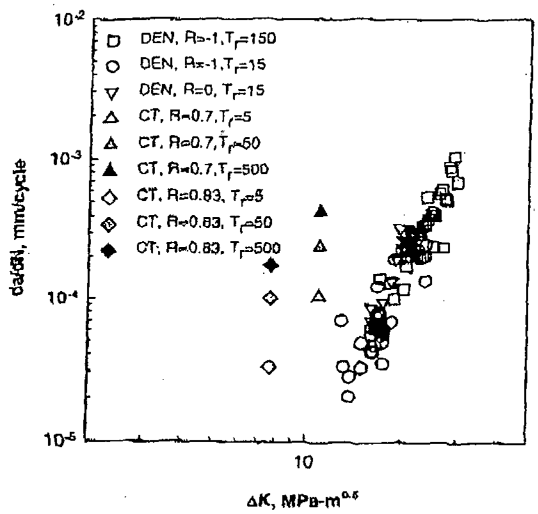

Fig. 7 304 SS crack growth rates in water at 288 °C. Rise time (T_r) is in seconds

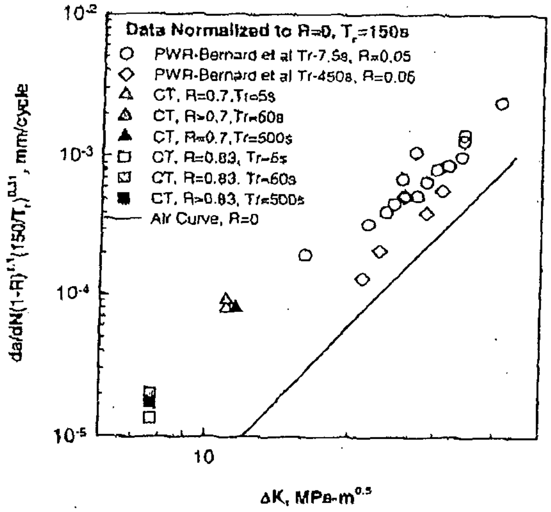

Fig. 9 Normalized 304 SS CT FCP Data at Low Potential. Normalization: $(1-R)^{-1.1}$, $T_r^{0.31}$ to $R=0, T_r=150$ s

The results in Fig. 7 indicate a strong effect of both T_r and R. The environmental effects can be rationalized in terms of a combined mean stress effect on closure or R ratio and a rise time or frequency effect, consistent with the literature. Bamford [22] noted larger environmental effects at higher R ratios. He incorporated an effective $\Delta K_{eff}=K_{max}(1-R)^{0.5}$, which shifted the high R data more in line with low R data. Cullen [23] reported strongly increased FCP rates for cast stainless steel at higher R in PWR water. The data by Bernard et al. [24] on Z3 CND17-12, similar to 316 SS, showed a clear rise time effect in PWR water. Recently, a correlation for FCP of austenitic stainless steels in BWR water was developed by Itatani et al. [25]. The correlation was of the form

$$da/dN=A(\Delta K)^m T_r^n/(1-R)^p \quad \text{with } m=3.0,$$
$$n=0.5, \text{ aidand } p=2.12 \tag{4}$$

This formulation indicates a strong role of T_r and R, consistent with results described above in low oxygen water. It is noted that the present crack growth rates are similar to those reported by Itatani et al. [25] in BWR water in the few cases where data are available at similar T_r, R, and ΔK. Figure 8 shows that the crack growth rates in Fig. 7 can be reasonably well normalized by $T_r^{0.31}$ and $1/(1-R)^{1.1}$. Hence, the form of the correlation developed by Itatani et al. for tension-tension appears to be promising for tension-compression. Further, the present rise time and stress ratio R ratio dependence are consistent with all but the very high R (0.95) BWR water data utilized by Itatani et al. [25]. Figure 9 shows that normalization in Fig. 8 worked successfully on data from compact tension tests at high R by Evans and Wire [2] and at low R by Bernard et al. [24]. Both data sets include long rise times (450–500 s) where environmental effects are substantial. The plot shows that ER reduces to about 2× at large ΔK. While the selected parameters values correlate these limited data sets, much more data would be required to obtain a definitive correlation.

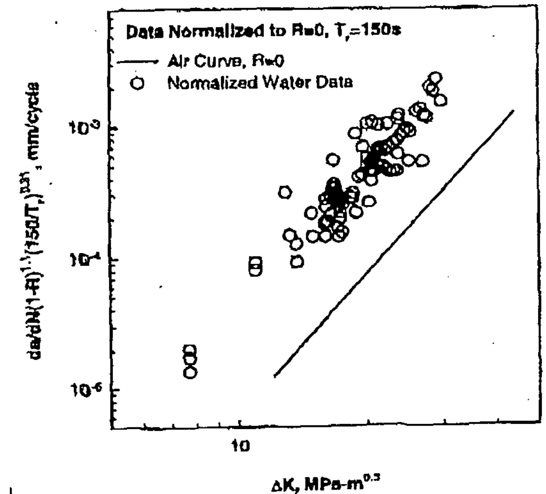

Fig. 8 Normalized 304 SS FCP Data vs ΔK [illegible]

4 Characterization of Fatigue Crack Propagation Mechanisms

Fracture surface features for specimens tested in air and water were evaluated to correlate operative cracking mechanisms with environmental cracking behavior. The fracture surface appearance for specimens tested in room temperature air was found to be dependent on loading conditions. A faceted morphology (Fig. 10(a)) was observed at crack growth rates less than 1×10^{-4} mm/cycle, vast fields of well-defined striations were generated between 1×10^{-4} and 1×10^{-3} mm/cycle, and a combination of fatigue striations and dimples (Fig. 10(b)) was observed above 1×10^{-3} mm/cycle. The nature of striated fracture surfaces in the intermediate and high crack growth rate regimes resembles that typically observed in FCC materials, but the facets formed at low crack growth rates are rather unique, as discussed below. Evidence of rubbing and fretting (Fig. 11) due to repeated contact between mating fracture surfaces was observed in specimens tested under fully reversed cyclic loading conditions.

Facets generated at low crack growth rates had an irregular appearance that was associated with a quasi-cleavage mechanism

... vs ΔK. Normalization: $(1-R)^{-1.1}\,T_r^{0.31}$ to $R=0$, $T_r=150$ s

that was operative for both shallow and deep cracks, as long as crack growth rates were less than 1×10^{-4} mm/cycle. Because

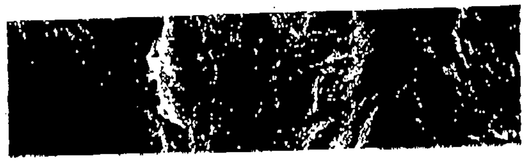

Fig. 10 Fractographs of 304 SS tested in 24°C air. (a) Irregular quasi-cleavage facets at $da/dN = 8\times10^{-5}$ mm/cycle. Arrow denotes failed twin boundary. (b) Striations and dimples at 1×10^{-2} mm/cycle

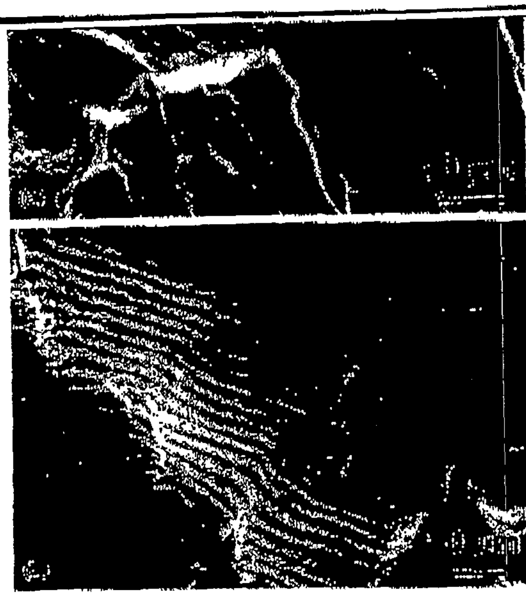

Fig. 11 Repeated contact between crack surfaces ($R = -1$). (a) Rub marks at low ΔK levels in 288°C air. (b) Striations surrounded by severely rubbed regions (24°C air).

304 SS is a metastable alloy at room temperature, the material directly ahead of an advancing crack undergoes a strain-induced transformation to α' martensite. Therefore, cracks propagate through martensite, which results in a quasi-cleavage morphology that resembles the quasi-cleavage fracture surface appearance in martensitic steels. Ferritescope measurements showed that all fatigue fracture surfaces generated at room temperature contained α' martensite, with the amount of martensite increasing at higher stress intensity factor levels due to larger plastic zone sizes.

The morphology of the quasi-cleavage facets was consistent with the fracture surface appearance for 304 SS (Gao et al. [26]) and high purity Fe-18Cr-12Ni SS (Wei et al. [27]) tested in room temperature air, 3.5% NaCl solutions and hydrogen. Strain-induced α' martensite formed ahead of fatigue cracks in both alloys, which caused a quasi-cleavage mechanism. Unlike 304 SS, 316 SS fatigue tested in room temperature air (Mills [28]) exhibited more conventional, cleavage-like facets. Because 316 SS is a more stable alloy due to its higher nickel content, α' martensite transformation does not occur at room temperature; hence, it exhibits classic, cleavage-like faceted growth as cracks propagate through stable austenite.

In the low crack growth rate regime, 304 SS also exhibited localized cracking along annealing twin boundaries, but no evidence of intergranular cracking. Localized separation along favorably oriented twin boundaries produced flat, featureless facets that appear as dark islands, surrounded by quasi-cleavage facets. Gao et al. [26] and Wei et al. [27] also reported twin boundary cracking in 304 SS and high purity Fe-18Cr-12Ni SS.

Facets formed in 288°C air had a different morphology, as they took on a more conventional cleavage-like appearance. Comparison of Figs. 12(a) and 12(b) shows that the high temperature facets had more of a cystallographic nature with some evidence of river patterns, in contrast with the irregular facets generated in room temperature air. The lack of quasi-cleavage facets indicates that 288°C is above the critical temperature where cold working induces a martensite transformation (i.e., M_D temperature). Based on the composition of 304 SS, the M_D temperature associated with 30% cold work is on the order of 100°C (Lacombe [29]). Indeed, Ferritescope measurements showed no detectable α'-martensite on fatigue fracture surfaces generated at 288°C.

At crack growth rates slightly above 1×10^{-4} mm/cycle, facets formed in 288°C air were poorly defined and parallel fracture markings associated with slip offsets were often superimposed on them. The transition to poorly defined facets is believed to be associated with a transition from heterogeneous-to-homogeneous slip. Fracture surfaces generated in 288°C water were remarkably different than those generated in air. Facets formed in water had a crystallographic appearance with well-defined river patterns, as shown in Fig. 12(c). The sharp, cleavage-like facets formed immediately adjacent to machined notches and well away from the notches, indicating that the same faceted growth mechanism was operative for shallow and long cracks. Moreover, well-defined crystallographic facets persisted over the entire range of crack growth rates generated in this program, including crack growth rates as high as 8×10^{-4} mm/cycle where fracture surfaces generated in air exhibited poorly defined facets and vast fields of fatigue striations. There was no evidence of either intergranular cracking or annealing twin boundary cracking in 288°C water.

Although fracture surfaces generated in 288°C water exhibited crisp cleavage-like facets, high magnification of facet faces revealed the presence of fatigue striations (Fig. 13). At crack growth rates from 1×10^{-4} to 3×10^{-4} mm/cycle, parallel fracture mark-

06/01/2008 19:59 3017623511 NOVERFLO PAGE 04

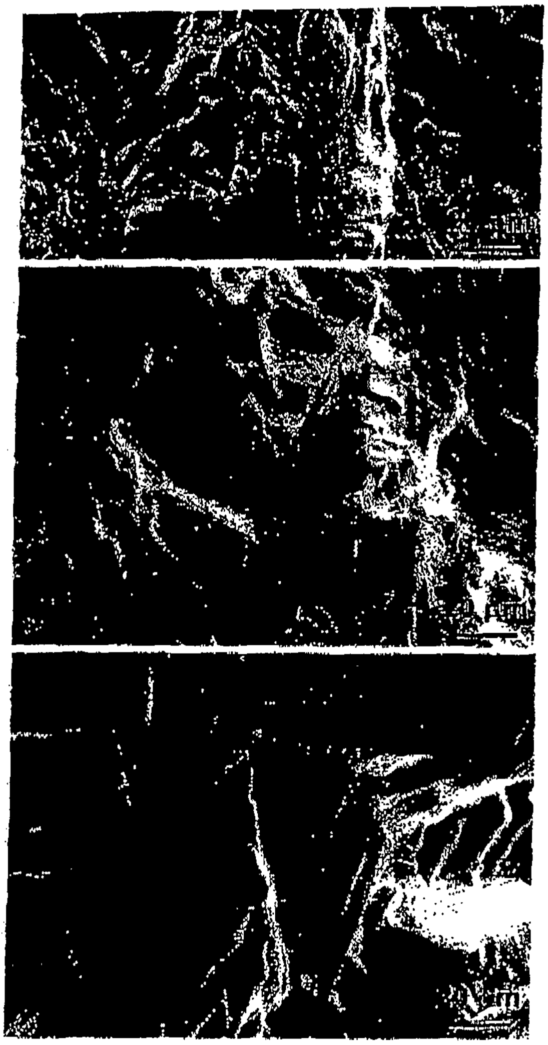

Fig. 12 Fractographs of 304 SS fatigue tested in (a) 24°C air showing irregular facets (b) 288°C air showing cleavage-like facets (c) 288°C water with crystallographic facets that are sharp, cleavage-like, and highly angular.

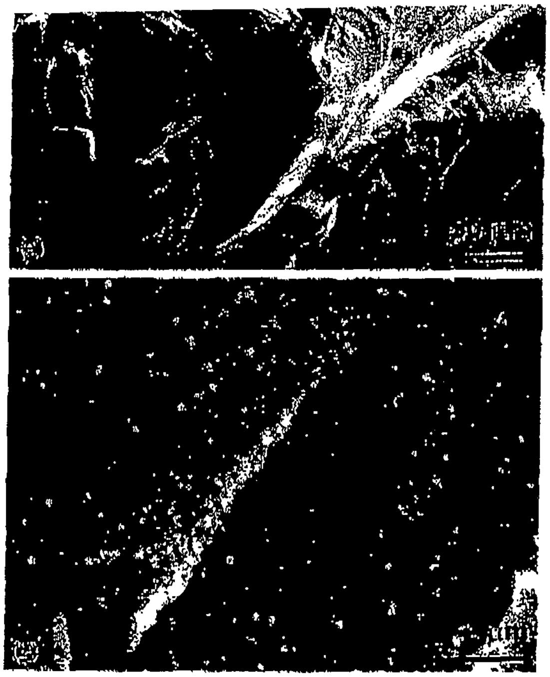

Fig. 13 Fractographs of 304 SS fatigue tested in 288°C water. (a) Highly angular faets persist to 3×10^{-4} mm cycle. (b) High magnification of (a) shows fatigue striations superimposed on facet faces

ings on the facets were very straight, but their spacing was identical to macroscopic crack growth rates indicating that they were fatigue striations. At growth rates above 3×10^{-4} mm/cycle, striations had a ductile or wavy appearance, as shown in Fig. 13(b).

Facet and striation orientations on fracture surfaces generated in 288°C water revealed that local cracking directions were often very different from the overall cracking direction. Although facets were usually aligned in the cracking direction, some were aligned normal to the macroscopic cracking direction (Figs. 12(c) and 13(a)). Likewise, most striations were oriented normal to overall cracking direction, but in some regions striations had different orientations and in some cases were even parallel to the macroscopic cracking direction. These observations indicate that crack advance in water involved a very uneven process, as cracking first occurred in the most susceptible regions, which left ligaments in the wake of the advancing crack front. As the overall crack continued to extend, local stress intensities within the more resistant ligaments increased to the point where cracking reinitiated and propagated across the ligaments. As a result, local cracking directions within these ligaments were often normal to the overall cracking direction. The rapid crack advance in the more susceptible regions is believed to be a significant contributor to the environmental acceleration observed in high temperature water. Specifically, this rapid cracking not only increased the overall crack length, it increased local stress and provided alternate paths for reinitiating local cracks along the more resistant ligaments.

The role of active path dissolution versus hydrogen embrittlement in causing accelerated cracking of stainless steel in high temperature water remains an issue because of the coupled nature of these processes, as electrochemical reactions near the crack tip involve both anodic dissolution of the metal and a cathodic reaction that produces hydrogen. The presence of well-defined crystallographic features indicates the absence of significant metal dissolution, thereby suggesting that slip/dissolution is not the primary cause of accelerated cracking. This observation is consistent with findings by Chopra and Smith [10] that crack growth rates for 304 SS are greater in low dissolved oxygen water than in high dissolved oxygen water. This observation cannot be reconciled with a slip/dissolution mechanism.

The presence of sharp, crystallographic facets suggests that a hydrogen embrittlement mechanism is responsible for accelerated cracking in 288°C water. This is supported by fractographic findings by Hanninen and Hakarainen [30] where hydrogen-precharged 304 SS exhibited cleavage-like facets without any detectable α' martensite formation. The facet morphology for the hydrogen-precharged specimens is very similar to that observed in 288°C water, thereby implicating hydrogen in promoting accelerated cracking in high temperature water. Moreover, Gao et al. [26] and Wei et al. [27] demonstrated that a hydrogen embrittlement mechanism was responsible for accelerated fatigue crack growth rates in stainless steel alloys tested in room temperature aqueous environments. Although α' martensite formation occurred in these specimens, Gao and Wei determined that this transformation did not have a critical role in controlling crack growth rates and it was not a prerequisite for hydrogen embrittlement.

Although hydrogen embrittlement is believed to be the primary cause of environmental cracking in 288°C water, it is possible that oxide film formation at the crack tip also affects cracking behavior by restricting slip reversals during the unloading portion of fatigue cycles. The importance of oxide film formation in affecting fracture surface morphology is apparent when comparing fracture surfaces generated in air and vacuum. Fatigue fracture surfaces generated in air possessed crystallographic facets, whereas those generated in vacuum had a nondescript, nonfaceted appearance (Wire [1]). Apparently, the thin oxide film that forms in 24°C air serves as a dislocation barrier that impedes slip reversals during unloading cycles. Hence, damage tends to be concentrated along particular slip bands, and eventually local separation along these slip bands produces crystallographic facets. In vacuum, the absence of an oxide film promotes more effective slip reversals that minimizes local damage along any particular slip band. As a result, crystallographic facets do not develop in vacuum. Oxide film formation in water is also expected to restrict slip reversals and promote facet formation and higher crack growth rates; however, the degree of acceleration is expected to by much less than that associated with hydrogen embrittlement.

In summary, it is unlikely that slip/dissolution is a primary cause of environmental cracking in 288°C hydrogenated water because of the presence of crisp crystallographic features and an increase in crack growth rates with decreasing dissolved oxygen levels (Chopra and Smith, [10]). The cleavage-like facets on the fracture surface, which are very similar to facets found in hydrogen-precharged 304 SS (Hanninen and Hakarainen [30]), suggest that hydrogen embrittlement is the primary cause of accelerated cracking in high temperature water. It is also likely that the formation of crack tip oxides restricted slip reversals which also contributed to increased crack growth rates, although this effect is expected to be much smaller effect than that associated with hydrogen embrittlement.

5 Summary and Conclusions

Instrumented corrosion fatigue tests on 304 SS DEN specimens provided fatigue crack growth rate data in 24° and 288°C air and 288°C water over a wide range of crack growth rates. Results in air and water at the same mechanical parameters allowed direct assessment of environmental effects, avoiding any concerns for data variability due to materials, test technique, and data correlation. Crack growth rates in water are about 12× times the air rate at low speeds where the environmental effects are largest. The large environmental degradation in crack growth is consistent with the strong reduction of fatigue life in commercial PWR water. Further, very similar crack growth rate data were reported in low oxygen HWC, in both surface crack and conventional deep crack tests. The large environmental enhancement in 304 SS (12×) persisted to crack extensions up to 4.1 mm, far outside the range associated with short crack effects. The same large environmental effects observed in the DEN tests were reproduced in CT specimens at a high stress ratio and low ΔK. The overall results can be normalized successfully by incorporating the combined effects of stress ratio and rise time, qualitatively similar to the formulation developed by Itatani et al. to describe test results in BWR water.

Much of literature data in hydrogenated water chemistry shows an apparently mild environmental effect for 304 SS, with an ER of 2.55 or less. However, based on the current test results, larger environmental effects occur in hydrogenated water in the low ΔK regime at long rise times and high R-ratio conditions.

The high crack growth rates in 288°C deaerated water were associated with a faceted growth mechanism. The highly angular, cleavage-like appearance of the facets suggests that a hydrogen embrittlement mechanism was the primary cause of accelerated cracking in this environment.

Acknowledgment

This work was performed under U.S. Department of Energy Contract with Bechtel Bettis, Inc. The authors wish to acknowledge the efforts of H. K. Shen, A. J. Bradfield, J. T. Kandra, and J. J. Chasko in performance of these experiments.

References

[1] Wire, G. L., and Mills, W. J., 2001, "Fatigue Crack Propagation From Notched Specimens of 304 Stainless Steel in An Elevated Temperature Aqueous Environment," PVP-Vol. 439, *Pressure Vessel and Piping Codes and Standards-2002*, PVP2002-1232, ASME, New York, pp. 151–164.
[2] Evans, W. M., and Wire, G. L., 2001, "Fatigue Crack Propagation Behavior of 304 Stainless Steel From Compact Tension Specimens in An Elevated Temperature Aqueous Environment," PVP-Vol. 439, *Pressure Vessel and Piping Codes and Standards-2002*, PVP2002-1226, ASME, New York, pp. 91–98.
[3] Wire, G. L., Leax, T. R., and Kandra, J. T., 1999, "Mean Stress and Environmental Effects on Fatigue In Type 304 Stainless Steel," *Probabilistic and Environmental Aspects of Fracture and Fatigue*, PVP-Vol. 386, ASME, New York, pp. 213–228.
[4] Schijve, J., 1982, "The Stress Intensity Factor of Small Cracks at Notches," Fatigue Fract. Eng. Mater. Struct., 5(1), pp. 77–90.
[5] Tada, H., Paris, P. C., and Irwin, G. R., 2000, *The Stress Analysis of Cracks Handbook*, ASME.
[6] Yamamoto, Y., Sumi, Y., and Ao, K., 1974, "Stress Intensity Factors of Cracks Emanating From Semi-Elliptical Side Notches in Plates," Int. J. Fract., 10(4), p. 593.
[7] Newman, J. C., 1992, "Fracture Mechanics Parameters for the Small Fatigue Cracks," *Small-Crack Test Methods*, ASTM STP 1149, pp. 6–33.
[8] James, L. A., and Jones, D. P., 1985, "Fatigue Crack Growth Correlations for Austenitic Stainless Steels in Air," *Predictive Capabilities in Environmentally Assisted Cracking*, PVP Vol. 99, pp. 363–414.
[9] Lalor, P., Sehitoglu, H., and McClung, R. C., 1986, "Mechanics Aspects of Small Crack Growth From Notches-the Role of Crack Closure," *The Behavior of Short Fatigue Cracks*, EGF Pub. 1, K. J. Miller and E. R. de los Rios, eds., Mechanical Engineering Publications, London, pp. 369–386.
[10] Chopra, O. K., and Smith, J. L., 1998, "Estimation of Fatigue Strain-Life Curves for Austenitic Stainless Steels in Light Water Reactor Environments," *Fatigue, Environmental Factors, and New Materials*, PVP Vol. 374, ASME, New York, pp. 249–259.
[11] Scott, P. M., 1988, "A Review of Environmental Effects on Pressure Vessel Integrity," *Proceedings of the Third Environmental Degradation of Materials in Nuclear Power Systems-Water Reactors*, TMS, pp. 15–29.
[12] Shoji, T., Takahasi, H., Suzuki, M., and Kondo, T., 1981, "A New Parameter for Characterizing Corrosion Fatigue Crack Growth," ASME J. Eng. Mater. Technol., 103, pp. 298–304.
[13] Leax, T. R., 1999, "Statistical Models of Mean Stress and Water Environment Effects on the Fatigue Behavior of 304 Stainless Steel," *Probabilistic and Environmental Aspects of Fracture and Fatigue*, PVP Vol. 386, ASME, New York, pp. 229–239.
[14] Gangloff, R. P., 1985, "Crack Size Effects on the Chemical Driving Force for Aqueous Corrosion Fatigue," Metall. Trans. A, 16A, pp. 953–969.
[15] Shack, W. J., and Kassner, T. F., 1994, "Review of Environmental Effects on Fatigue Crack Growth of Austenitic Stainless Steels," NUREG/CR-6176, ANL-94/1.
[16] Prater, T. A., Catlin, W. R., and Coffin, L. F., 1985, "Effect of Hydrogen Additions to Water on the Corrosion Fatigue Behavior of Nuclear Structural Materials," *Proceedings of the Second International Symposium on Environmental Degradation of Materials in Nuclear Power Systems-Water Reactors*, NACE, pp. 615–623.
[17] Gordon, B. M., Indig, M. E., Davis, R. B., Pickett, A. E., and Jewett, C. W., 1985, "Environmentally Assisted Cracking Resistance of BWR Structural Materials in Hydrogen Water Chemistry," *Proceedings of the Second International Symposium on Environmental Degradation of Materials in Nuclear Power Systems-Water Reactors*, NACE, pp. 583–592.
[18] Jewett, C. W., and Pickett, A. E., 1986, "The Benefit of Hydrogen Addition to the Boiling Water Reactor Environment on Stress Corrosion Crack Initiation and Growth in Type 304 Stainless Steel," ASME J. Eng. Mater. Technol., 108, pp. 10–19.
[19] Ljungberg, L. G., 1989, "Effect of Water Impurities in BWR on Environmental Crack Growth Under Realistic Load Conditions," *Proceedings of the*

Fourth International Symposium on Environmental Degradation of Materials in Nuclear Power Systems-Water Reactors. NACE, pp. 4-59–4-75.

[20] Andresen, P. L., and Campbell, P. G., 1989, "The Effects of Crack Closure in High Temperature Water and Its Role in Influencing Crack Closure Data," *Proceedings of the Fourth International Symposium on Environmental Degradation of Materials in Nuclear Power Systems-Water Reactors*, Jekyll Island, NACE, pp. 4-86–4-110.

[21] Gilman, J. D., 1988, "Corrosion-Fatigue Crack-Growth Rates in Austenitic Stainless Steels in Light Water Reactor Environments," Int. J. Pressure Vessels Piping, 31, pp. 55–68.

[22] Bamford, W. H., 1979, "Fatigue Crack Growth of Stainless Steel Piping in a Pressurized Water Reactor Environment," ASME J. Pressure Vessel Technol., 101, pp. 73–79.

[23] Cullen, W. H., 1985, "Fatigue Crack Growth Rates of Low-Carbon and Stainless Piping Steels in PWR (Pressurized Water Reactor) Environment," NUREG/CR-3945, MEA-2055.

[24] Bernard, J. L., Slama, G., and Rabbe, P., 1979, "Influence of PWR Environment on Fatigue Crack Growth Behavior of Stainless Steels," *Time and Load Dependent Degradation of Pressure Boundary Materials*, IWG-RRPC-79/2, International Atomic Energy Agency, pp. 27–36.

[25] Itatani, M., Asano, M., Kikuchi, M., Suzuki, S., and Iida, K., 2001, "Fatigue Crack Growth Curve for Austenitic Stainless Steels in BWR Environment," ASME J. Pressure Vessel Technol., 123, pp. 166–172.

[26] Gao, M., Chen, S., and Wei, R. P., 1992, "Crack Paths, Microstructure, and Fatigue Crack Growth in Annealed and Cold-Rolled AISI 304 Stainless Steels," Metall. Trans. A, 23A, pp. 355–371.

[27] Wei, R. P., and Gao, M., 1993, "Micromechanism for Corrosion Fatigue Crack Growth in Metastable Austenitic Stainless Steels," *Corrosion-Deformation Interactions*, Les Editions de Physique, Les Ulis, France, pp. 619–629.

[28] Mills, W. J., and James, L. A., 1988, "Fatigue Crack Propagation Behavior of Type 316 Stainless Steel at Elevated Temperature in a Vacuum," Int. J. Fatigue, 10, pp. 33–36.

[29] Lacombe, P., and Beranger, G., 1993, "Structure and Equilibrium Diagrams of Various Stainless Steel Grades," *Stainless Steels*, Les Editions de Physique, Les Ulis, France, pp. 15–58.

[30] Hanninen, H., and Hakarainen, T., 1980, "On the Effects of α' Martensite in Hydrogen Embrittlement of a Cathodically Charged AISI Type 304 Austenitic Stainless Steel," Corrosion (Houston), 36, pp. 47–51.